# Novel method for manufacturing optical fiber: extrusion and drawing of microstructured polymer optical fibers from a 3D printer

WANVISA TALATAISONG,[1,*] RAND ISMAEEL,[1,2] SEYED REZA SANDOGHCHI,[1] TEERAPAT RUTIRAWUT,[1] GLENN TOPLEY,[1] MARTYNAS BERESNA,[1] AND GILBERTO BRAMBILLA,[1]

[1]*Optoelectronics Research Centre, University of Southampton, Southampton, SO17 1BJ, UK*
[2]*National Oceanography Centre, Southampton, SO14 3ZH, UK*
*\* w.talataisong@soton.ac.uk*

**Abstract:** Microstructured polymer optical fibers (MPOFs) have long attracted great interest due to their wide range of applications in biological and chemical sensing. In this manuscript, we demonstrate a novel technique of manufacturing MPOFs via a single-step procedure by mean of a 3D printer. A suspended-core polymer optical fiber has been extruded and directly drawn from a micro-structured 3D printer nozzle by using an acrylonitrile butadiene styrene (ABS) polymer. Near-field imaging at the fiber facet performed at the wavelength $\lambda \sim 1550$ nm clearly indicates guidance in the fiber core. The propagation loss has been experimentally demonstrated to be better than $\alpha = 1.1$ dB/cm. This work points toward direct MPOFs manufacturing of varieties of materials and structures of optical fibers from 3D printers using a single manufacturing step.

## 1. Introduction

Microstructured optical fibers (MOFs) have attracted an increased interest because of their wide range of unique properties such as ultrawide single mode operation, tailorable dispersion, high or low nonlinearity, and guidance in selected spectral regions. These features promoted MOF in numerous applications in telecoms, power delivery systems, industrial lasers, environmental monitoring as well as medicine/healthcare. The use of polymers as material of choice has been proposed to reduce manufacturing cost and increase the fiber mechanical ductility for applications in environments exposed to vibrations. Many techniques have been suggested and implemented to fabricate microstructured polymer optical fibers (MPOFs) and their related preforms, including stacking, drilling, milling, and polymerization of liquid monomers [1, 2]. Yet, these conventional techniques have limitations to the number of transverse features or the hole shapes, and it often involves multiple steps and requires expensive facilities like clean-room environment for fabrication.

A promising alternative to the conventional preform drawing is represented by billet extrusion, which has been shown to be a versatile, reproducible single-step approach for the fabrication of soft glass and polymer structured optical fiber preforms [3-7]. Preforms are fabricated by forcing a soft bulk polymer billet through a die to form a preform with a complex transverse profile. Non-circular holes, large air-filling fractions, and long preforms can be achieved with this technique. This technique, however, does not draw optical fibers directly, and thus is limited to manufacture only the preforms.

In the past decade, additive manufacturing has gained interest in many applications of optical device fabrication. In particular, 3D printing has shown strong potential for the manufacture of optical waveguides in many regions of the optical spectrum, including telecom, mid-infrared and terahertz [8-13]. Since devices operating in the terahertz region require dimensions comparable to the width of the 3D printed structures, hollow-core MPOFs were directly 3D printed without any subsequent drawing [12]. Simultaneously, the fabrication of

solid core optical fibers drawn from 3D printed preforms has been investigated [14]. A step-index plastic fiber has been drawn in 2016 from a fiber preform printed using a two-nozzle 3D printer with acrylonitrile butadiene styrene (ABS) and Polyethylene Terephthalate Glycol (PETG) filaments [15]. This fiber showed the possibility of guiding light at telecom wavelengths. A year later, the first drawn hollow-core fiber (HCF) cane based on the 3D printed preform was demonstrated, but no guiding was observed. Both circular and rectangular hollow-core fiber preforms were 3D printed using ABS filaments [16]. The first 3D printed hollow-core fiber guiding in the mid-IR has been also proposed in the same year [17]: and guidance in the mid-IR ( $\lambda$=3.5 – 5 µm) has been confirmed.

3D printers have been optimized for printing high quality objects from a variety of materials including polymers, glasses, and metals, resulting in improved control systems which include built-in temperature controller and polymer filament feeding system, allowing for their potential use in fiber drawing. By combining the extrusion technique with the capabilities of 3D printers, the extrusion of coreless solid optical fibers in one low-cost process has been shown [18].

Here we present the fabrication of a MPOF in a single step using a desktop fused deposition (FDM) 3D printer as the extruder. A suspended-core fiber was extruded and directly drawn from a structured nozzle. Consequently, our approach is much faster than printing the preform and extruding it afterwards. Also the length of extruded fiber in principle can be limited only by the length of the filament. The fiber microstructure was maintained all along the fiber allowing to demonstrate light guiding.

## 2. Structured nozzle design and fiber fabrication

Suspended core fiber is chosen for extruding MPOF because of its relatively simple geometry, which allows to fabricate light guiding fiber using a single material. 3D models of the nozzle with the fiber cross section inverse structure profile was designed with the Fusion 360, Autodesk software and were used for computer numerical control (CNC) machining. The nozzle was manufactured using a micromachining technique, traditionally used to fabricate the dies used for extruding structured fiber preforms. The design of structured nozzles is separated into two pieces including the nozzle body and the nozzle cover. Figure 1(a) reveals the designed structured nozzle including a 3D model, and side- and bottom-view cross-sections.
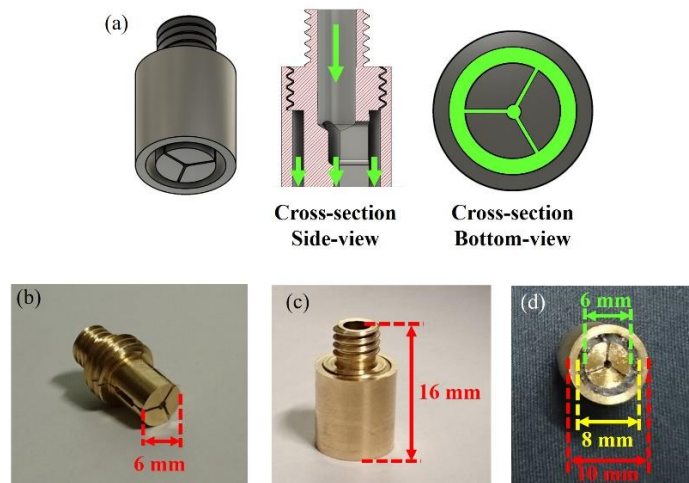


Fig.1 (a) Structured nozzle design including a 3D model, a side- and a bottom-view cross-sections, from left to right respectively. Green arrows and green colours represent the direction of filament moving and cross-section of extruded polymer from structured nozzle. (b-d) Micromachined structured nozzle: (b) body, (c) body + cover, (d) after MPOF drawing.

To extrude the fiber, the machined nozzle was mounted on the printing head and a commercially available 3D printer filament (acrylonitrile butadiene styrene (ABS)) was fed through it. The extrusion quality was tested by extruding the fiber preform without any additional drawing. Different extrusion parameters (feeding speed and nozzle temperature) were used to explore their impact on the quality of the extruded preform and achieve the optimal effective temperature experienced by the polymer during drawing.

When the filament feeding speed was $s$~100 mm/min and the nozzle temperature $T$~250 ℃, air bubbles occurred in the extruded preform and a coarse surface was be observed. To reduce the size and number of bubbles, $T$ was decreased from 250 ℃ to 230 ℃ but large number of bubbles and surface non-uniformities still remained. These bubbles were attributed to the expansion of air trapped in the filament due to high filament $T$ inside the nozzle. These bubbles are extremely detrimental and can result in a deformation of the microstructure inside the fiber and cause the fiber to break at small diameters. When $s$ was changed, slow feeding speeds, resulted in low filament fictive temperature thus affecting the surface quality of the extruded structure. When the $s$ was increased to 250 mm/min, a smooth surface was achieved.

The surface roughness and defect formation in the extruded polymeric structure are strongly dependent on the fictive temperature. For $T$~250 ℃, a smooth and shiny surface was observed, but defects inside structure appeared, attributed to the presence of bubbles. At $T$~240 ℃, both surface roughness and bubble formation were reduced. Matt surface was observed at $T$ ~ 230 ℃ and was attributed to instabilities in the polymer flow behavior as a result of the wall slippage. The average surface roughness (Ra) of the extruded preforms were measured by importing (Fig.2) into a surface characterization software (Gwyddion). Results show that Ra of the preforms extruded at speed of 100 mm/min and 250 mm/min are 249.6 nm and 91.8 nm, respectively. A comparison between surface roughness of extruded preforms with feeding speeds of 100 mm/min and 250 mm/min (at the same nozzle temperature of 240 ℃) is shown in Fig. 2.
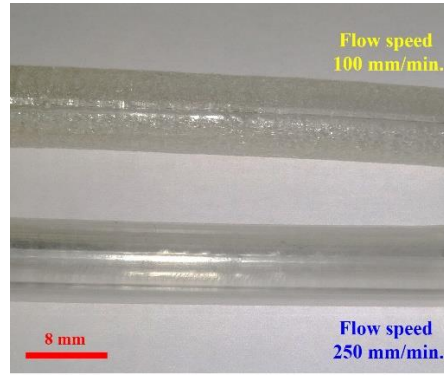


Fig. 2 Extruded structures with different filament feeding speeds at $T$= 240 ℃.

The polymer fiber was extruded at $T$ ~ 240 ℃ through the structured nozzle at $s$ ~ 250 mm/min by using a built-in feeding motor [Figs. 3(a)-3(b)]. Diameter reduction (fiber drawing) took place by connecting the extruded polymer fiber preform to a constantly rotating spool. A stepper motor was used to rotate the spool and the pulling speed of fiber drawing was controlled by changing the rotation speed ($\Omega$) of the stepper motor [Figs. 3(c)-3(d)].

The suspended-core polymer optical fiber was directly drawn from the 3D printer structured nozzle at $\Omega$ ~20 rpm. The final diameter of drawn MPOF was $d$~800 µm. The MPOF was cleaved by using a heated razor blade and optical microscope images of different cross-sections showed that the microstructure inside fiber was maintained after drawing [Figs. 4(a)-4(b)]. The

surface roughness in the extruded preform was reduced by the fiber drawing. The different elliptical shape of fiber cross-section of Figs. 4(a) and (b) are caused by cleaving of the fiber.
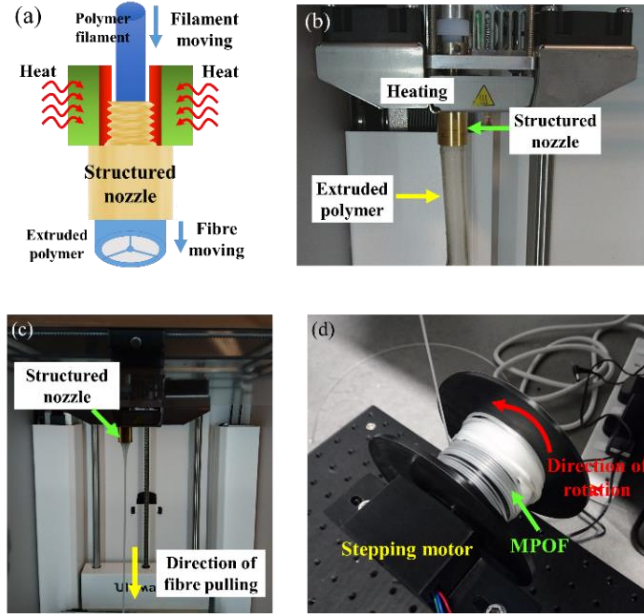


Fig.3 (a) Schematic and (b) photograph of the experimental setup used to extrude MPOF. (c) Fiber drawn from the heated structured nozzle. (d) MPOF wrapped onto the 3D printed spool connected to the stepper motor.
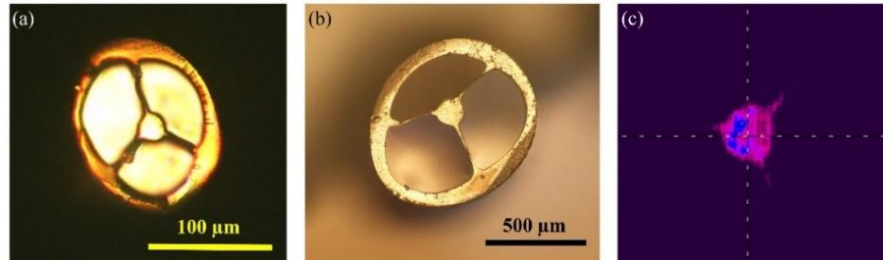


Fig. 4 (a,b) Microscope images of the fiber cross-section at different diameters. (c) Near field image ($\lambda$ = 1550 nm) at the fiber output for a full turn bending (R~12.5 mm)

## 3. Characterization of the suspended-core MPOF

In order to evaluate the MPOF optical guidance properties, the near-field image of the transmitted light at $\lambda$~1550 nm from the fiber facet was recorded. A fiberized laser source (Thorlabs, CLD1015) was launched into a 20 cm long section of fiber using a bare-fiber adapter. The image of the output intensity profile was taken by collecting the output of the fiber shown in Fig. 4(b) into a near-IR camera (Electrophysics, 7290A) using an objective lens with a 20 mm focal length.

The near field image of the fiber output was captured at different bending radii and confirmed guiding in the fiber core [Fig. 4(c)]. This not only corroborates that the fiber successfully guides light in the core, but it also demonstrates that no scattered light is guided in the cladding. In this experiment, the MPOF length was 5 m, but the fiber structure collapsed

after 50 cm. This collapse depends on the drawing parameters such as drawing speed, temperature, and air pressure inside the fiber cavities. Due to the fiber structure deformation, 20 cm of MPOF were used to characterize the propagation loss. An optical side scattering radiometry (OSSR) technique [19-21] was used to measure the fiber attenuation by using an integrating sphere (Newport 819D-SL-2). In this setup, light from the fiberized laser source with $\lambda = 1557$ nm was launched into the MPOF. Then, the optical fiber was inserted into the integrating sphere and the scattered light coming out from the fiber side was collected by the sphere on a detector as shown in Fig. 5(a). The scattered light at different sections of the fiber was measured by scanning the integrating sphere along the fiber (in 1 mm steps) over the length of 2.0 cm and confirmed a propagation loss of 1.1 dB/cm at $\lambda = 1557$ nm [Fig. 5(b)]. Attenuation was measured close to the input of fiber and included spurious values of radiation and high order modes that were still guided over this transition region. Therefore, lower attenuation is expected at longer fiber lengths. Also, the surface roughness of a fiber core can contribute to the high propagation loss. This can be improved by smoothening the inner surface of the nozzle die and by reducing the structural deformations associated to the fiber drawing.

Bend loss measurements were performed with different bend radii of 51.7, 80, 112.1 and 179.4 mm. As before, light from the fiberized laser source was coupled into a section of MPOF and the intensity at the optical fiber output at different bend radii was measured using a power meter. From the experimental results presented in Fig. 5(c), the bend loss at $\lambda = 1550$ nm for R~ 51.7 mm was estimated to be 20 dB/m.
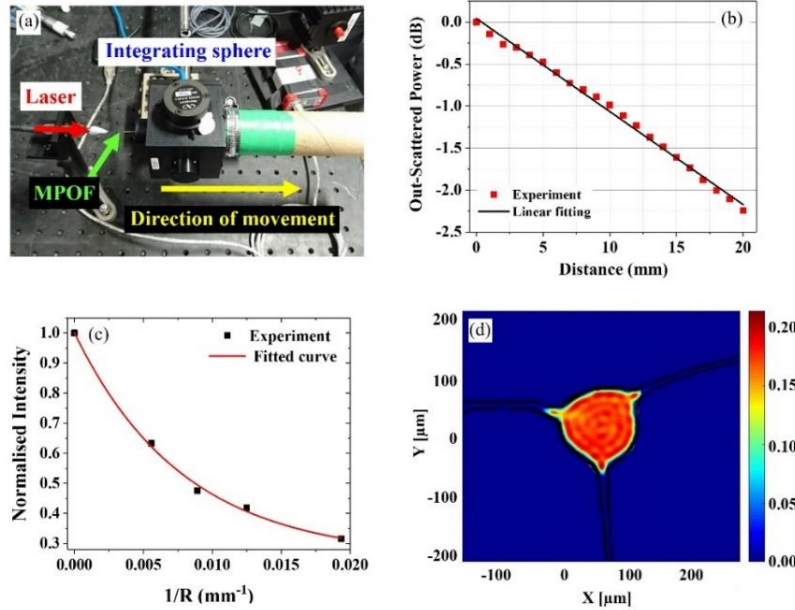


Fig. 5 (a) Experimental setup used to measure propagation loss, (b) Relationship between OSSR scattered power at $\lambda = 1557$ nm and distance, (c) Normalized transmitted intensity at different bend radii (R) at $\lambda = 1550$ nm. (d) Intensity profile of the mode supported by fiber core in the simulated fiber structure at $\lambda \sim 1550$ nm.

Simulations of the mode propagating through the extruded and drawn suspended-core MPOFs were performed by importing the microscope image cross-section [Fig. 4(b)] of the fiber used for loss measurements into a commercial finite element method software (Lumerical©). Figure 5(d) shows the intensity distribution of a linear combination of equally weighted supported mode at $\lambda \sim 1550$ nm. This result is consistent with the experimental result of Fig. 4(c), where light is mostly confined in the fiber core and there is a small overlap with the three struts. The different intensity distribution between experiments and simulations are

attributed to the mode mismatch between the light source and the fiber, which resulted in an unpredictable weight distribution between the various modes guided in the core. Bending could also cause the different weight and number of propagating modes. Indeed, the fiber is heavily multimoded (more than 70 modes) at $\lambda \sim 1550$ nm, due to the large fiber core, and the leaking into three struts around fiber core, observed in both experimental and simulated result, can be attributed to high order modes, such as $HE_{94}$. Single mode operation can be achieved in a fiber with a smaller core size, which could be manufactured by pressurizing the air holes around the fiber core and optimizing the drawing speed to reach a regime driven by viscosity and not by surface tension. The drawing parameters and optical properties of first MPOF directly drawn from a 3D printer is presented in Table 1.

Table 1. Conclusion of MPOF drawing parameters, fiber geometry and optical properties

|  | MPOF material and drawing parameters | MPOF geometry | MPOF optical properties |
|---|---|---|---|
| Material | ABS |  |  |
| Feeding speed (mm/min) | 250 |  |  |
| Temp (ºC) | 240 |  |  |
| Drawing speed (rpm) | 20 |  |  |
| Core diameter (µm) |  | 133 |  |
| Fiber diameter (µm) |  | 800 |  |
| Bending loss (dB/m) |  |  | 20 |
| Attenuation (dB/cm) |  |  | 1.1 |

## 4. Conclusion

In conclusion, a direct drawing of a microstructured polymer optical fibers from a low-cost desktop 3D printer has been demonstrated. Given the relatively small cost and short time of operation of current desktop printers compared with a conventional drawing tower, this could become an invaluable tool for the fabrication of microstructured optical fibers. Images of the final fiber cross-section indicate the possibility of maintaining the microstructure inside the fiber after the drawing process. Although the size of fiber is large compared with commercial optical fibers (Ø 125 µm), this demonstrates the potential to directly draw microstructured polymer optical fiber using a customized 3D printer head. The near-field end facet image and the modal profile simulations show the ability to confine light at $\lambda \sim 1550$ nm in the fiber core. The measured maximum propagation loss reveals an attenuation of 1.1 dB/cm at $\lambda \sim 1557$ nm. A natural next step can be designing the nozzle die for different optical fiber geometries. The developments in new 3D printer filaments made of different polymers or even soft glasses can be envisaged. 3D printing can provide a cost-effective production process, both in terms of polymer preform and optical fibers, compared to conventional high-cost and lengthy two-step fabrication methods.

## References

1. M. A. v. Eijkelenborg, M. C. J. Large, A. Argyros, J. Zagari, S. Manos, N. A. Issa, I. Bassett, S. Fleming, R. C. McPhedran, C. M. d. Sterke, and N. A. P. Nicorovici, "Microstructured polymer optical fibre," Opt. Express **9**, 319-327 (2001).
2. Y. Zhang, K. Li, L. Wang, L. Ren, W. Zhao, R. Miao, M. C. J. Large, and M. A. v. Eijkelenborg, "Casting preforms for microstructured polymer optical fibre fabrication," Opt. Express **14**, 5541-5547 (2006).
3. H. Ebendorff-Heidepriem, T. M. Monro, M. A. van Eijkelenborg, and M. C. J. Large, "Extruded high-NA microstructured polymer optical fibre," Optics Communications **273**, 133-137 (2007).
4. H. Ebendorff-Heidepriem, P. Petropoulos, S. Asimakis, V. Finazzi, R. C. Moore, K. Frampton, F. Koizumi, D. J. Richardson, and T. M. Monro, "Bismuth glass holey fibers with high nonlinearity," Opt. Express **12**, 5082-5087 (2004).
5. X. Feng, T. M. Monro, V. Finazzi, R. C. Moore, K. Frampton, P. Petropoulos, and D. J. Richardson, "Extruded singlemode, high-nonlinearity, tellurite glass holey fibre," Electronics Letters **41**, 835-837 (2005).
6. J. Y. Y. Leong, P. Petropoulos, J. H. V. Price, H. Ebendorff-Heidepriem, S. Asimakis, R. C. Moore, K. E. Frampton, V. Finazzi, X. Feng, T. M. Monro, and D. J. Richardson, "High-Nonlinearity Dispersion-Shifted Lead-Silicate Holey Fibers for Efficient 1-um Pumped Supercontinuum Generation," J. Lightwave Technol. **24**, 183 (2006).
7. P. Petropoulos, H. Ebendorff-Heidepriem, V. Finazzi, R. C. Moore, K. Frampton, D. J. Richardson, and T. M. Monro, "Highly nonlinear and anomalously dispersive lead silicate glass holey fibers," Opt. Express **11**, 3568-3573 (2003).
8. V. A. S. Alice L. S. Cruz, Carmem L. Barbosa, and Marcos A. R. FrancoI, "3D Printed Hollow Core Fiber with Negative Curvature for Terahertz Applications," Journal of Microwaves, Optoelectronics and Electromagnetic Applications **14**, 9 (2015).
9. A. L. S. Cruz, A. Argyros, X. Tang, C. M. B. Cordeiro, and M. A. R. Franco, "3D-printed terahertz Bragg fiber," in *2015 40th International Conference on Infrared, Millimeter, and Terahertz waves (IRMMW-THz)*, 2015), 1-2.
10. K. C. J. Canning, Y. Luo, S. Leon-Saval, G-D. Peng, E. Comatti, M.A. Hossain, Z. Reid, "3D printing of optical fibre preforms," in *Asia Communications and Photonics Conference (ACP)*, (Hong Kong, 2015).
11. J. C. K. Cook, S. Leon-Saval, Z. Reid, M. A. Hossain, J. E. Comatti, Y. Luo and G-D. Peng, "Optical fibre fabricated from a 3D-printed preform," in *Australia NZ Conf. Optics & Photonics (ANZCOP)*, (Adelaide, Australia, 2015).
12. J. Li, K. Nallappan, H. Guerboukha, and M. Skorobogatiy, "3D printed hollow core terahertz Bragg waveguides with defect layers for surface sensing applications," Opt. Express **25**, 4126-4144 (2017).
13. J. C. K. Cook, "3D printed photonics," in *Asia Pacific Opt. Sensors (APOS2018)*, ( Matsue, Shimane, Japan, 2018).
14. K. Cook, J. Canning, S. Leon-Saval, Z. Reid, M. A. Hossain, J.-E. Comatti, Y. Luo, and G.-D. Peng, "Air-structured optical fiber drawn from a 3D-printed preform," Opt. Lett. **40**, 3966-3969 (2015).
15. K. Cook, G. Balle, J. Canning, L. Chartier, T. Athanaze, M. A. Hossain, C. Han, J.-E. Comatti, Y. Luo, and G.-D. Peng, "Step-index optical fiber drawn from 3D printed preforms," Opt. Lett. **41**, 4554-4557 (2016).
16. B. M. L. Thiago H. R. Marques, Jonas H. Osório, Luiz E. da Silva, Cristiano M. B. Cordeiro, "3D Printed Microstructured Optical Fibers," International Microwave and Optoelectronics Conference (2017).
17. W. Talataisong, R. Ismaeel, T. H. R. Marques, S. Abokhamis Mousavi, M. Beresna, M. A. Gouveia, S. R. Sandoghchi, T. Lee, C. M. B. Cordeiro, and G. Brambilla, "Mid-IR Hollow-core microstructured fiber drawn from a 3D printed PETG preform," Scientific Reports **8**, 8113 (2018).
18. J. Canning, M. A. Hossain, C. Han, L. Chartier, K. Cook, and T. Athanaze, "Drawing optical fibers from three-dimensional printers," Opt. Lett. **41**, 5551-5554 (2016).
19. D. B. K. F. P. Kapron, and R. D. Maurer, "Radiation losses in glass optical waveguides," Applied Physics Letters **17**, 423-425 (1970).
20. A. R. Tynes, A. D. Pearson, and D. L. Bisbee, "Loss Mechanisms and Measurements in Clad Glass Fibers and Bulk Glass," J. Opt. Soc. Am. **61**, 143-153 (1971).
21. S. R. Sandoghchi, M. Petrovich, D. R. Gray, Y. Chen, N. V. Wheeler, T. D. Bradley, N. H. L. Wong, G. T. Jasion, J. Hayes, E. N. Fokoua, M. B. Alonso, S. M. Mousavi, D. J. Richardson, and F. Poletti, "Optical side scattering radiometry for high resolution, wide dynamic range longitudinal assessment of optical fibers," Opt. Express **23**, 27960-27974 (2015).